# Hematite Nanoparticle-Modified Carbon Paper as a Promising Electrochemical Sensor for Atropine Detection in Beverages

Andrea Cabezas[a], Scarlett Aguilera[a,c], Sergio A. Urzúa[d], Christopher D. Cooper[d,e], Cristian Vera[a,c], María Aguirre[a,c*], Paulina Márquez[b,c*]and Jaime Pizarro[a,c*]

[a]Departamento de Química de los Materiales, Facultad de Química y Biología, Universidad de Santiago de Chile (USACH), Santiago, Chile.

[b]Escuela de Ingeniería, Universidad Central de Chile, 8330601, Santiago, Chile

[c]Millennium Institute on Green Ammonia as Energy Vector MIGA, ANID/Millennium Science Initiative Program/ICN2021_023.

[d]Department of Mechanical Engineering, Universidad Técnica Federico Santa María, Valparaíso, Chile.

[e]Centro Científico Tecnológico de Valparaíso, Valparaíso, Chile.

## Abstract

This study describes the electroanalytical determination of atropine in beverages using a carbon paper (CP) electrode modified with $Fe_2O_3$ nanostructures. The incorporation of nanoparticles of a transition metal oxide on CP led to an improvement in the electrochemical response of the electrode using the technique: square wave voltammetry (SWV). Morphological characterization of CPE/$Fe_2O_3$ developed by Field Emission Scanning Electron Microscopy (FESEM), shows a relatively uniform distribution of $Fe_2O_3$ nanoparticles on the CP surface. The optimization of variables of pH and the amount of modifying agent were relevant to maximize the efficiency of the modified electrode. The evaluation of the pH effect shows that the maximum current response occurs at pH 11.5 in Britton-Robinson buffer, and the optimum amount of $Fe_2O_3$ was 1 mg/mL, giving the best response, standing out for an optimum active surface for the detection of atropine. Electrostatic calculations show that at pH 11 the surfaces become negatively charged, having better affinity with protonated atropine, compared the deprotonated state. This pH is beyond atropine pKa, hence, the peak in current at pH 11.5 indicates that the surface induces a shift in pKa, allowing the prevalence of protonated atropine at this high pH. The limit of detection and quantification (LD and LQ) recorded using the CP/$Fe_2O_3$ electrode were 0.075 and 0.250 mM, respectively. In the case of real samples, using the standard addition method, the presence of interferents did not significantly affect the detection of atropine, obtaining satisfactory recovery percentages.

## 1. Introduction

Submission chemistry is a form of violence associated with criminal practices, especially sexual assault, robbery and fraud, which is generating more and more media coverage due to its social and health impact. In recent years, this phenomenon has become more relevant worldwide due to the increasing number of cases where psychoactive substances are used in drinks, particularly within the gastronomic sector (restaurants or bars) being able to introduce a deep depression of the level of consciousness, and therefore a submission with disinhibition and anterograde amnesia, leading a victim to perform acts against his or her will [1]. In many places, chemical submission has become a public health problem, affecting various sectors of the population [2]. In this context, there are different substances used for this type of crime and many of them are legal, but restricted in use, such as drugs with action on the central nervous system, such as benzodiazepines [3], and Z-drugs [4], however, there are also other illicit drugs that have a sedative effect and some hallucinogens, including cannabis, gamma hydroxybutyrate (GHB), lysergic acid (LSD), phencyclidine, among others [5]. Among the most common drugs used in chemical submission are tropane alkaloids, such as atropine, which are present in plants such as *Belladonna* and those derived from the *Solanaceae* family [6]. These substances are used in drugs, as they can act as stimulants or anticholinergics [7]. Atropine has a half-life of 4 hours [8], and therefore, when the victims make the report and go to a health center, they no longer find the presence of this alkaloid in their organism. Because of this, it is of major importance to have simple and rapid methods to detect the presence of this alkaloid in beverages, prior to consumption by the victim.

Atropine is a competitive antagonist of the muscarinic acetylcholine receptor and its chemical structure includes an ester group (tropic acid), an amino group and an aromatic group, unlike acetylcholine, which possesses an acetyl group and an ammonium group [6]. The mechanism of action of atropine and other related compounds is to compete with acetylcholine, which causes the binding of this neurotransmitter not to occur, thus attenuating physiological responses to parasympathetic nerve impulses [9]. Regarding its metabolic pathway, atropine is metabolized in the liver through hydrolysis and conjugation processes and excreted mainly in the urine [10] [11].

The most common methods used for atropine detection are chromatographic techniques, such as gas chromatography (GC) in combination with a mass spectrometer (MS) and is mainly used for the analysis of plant extracts and toxicological analysis [12], high performance liquid chromatography (HPLC) [13] and capillary electrophoresis (CE) [14], which are coupled with different detectors [15]. Although these techniques are effective, reliable, highly sensitive and selective, they are methods that require expensive equipment and reagents, highly trained personnel and need a relatively large physical space where they can be installed, not allowing on-site analysis. As an alternative to these techniques, electroanalytical techniques appear, which allow highly sensitive analyses with low detection limits, at a lower cost and without requiring sophisticated equipment, and with a much simpler operation. In this context, square wave voltammetry (SWV) is largely governed by the nature of the working electrode. The most common are mercury, gold, platinum and nowadays also carbon electrodes. The latter are relatively low cost and versatile, being able to interact with a wide range of measurable analytes. In general, these electrodes have significant limitations due to their slow surface kinetics, which considerably affects the sensitivity of the procedures [16].

There are several types of carbon working electrodes, among the most common are glassy carbon electrodes [17], carbon paste [18], among others. In the search for new carbon electrode surfaces, carbon paper (CP) stands out. Carbon paper electrodes are carbon fiber electrodes that are generally synthesized from a polymeric precursor corresponding to polyacrylonitrile (PAN) [19]. Carbon paper has large surface area, high surface-to-volume ratio, and porosity, which facilitate the diffusion of reactants [20]. Additionally, its relative high conductivity and low cost compared to conventional materials make it advantageous. Furthermore, its flexibility allows for adaptation to various sizes[19]. Carbon paper is widely used as electrodes in batteries [21] and fuel cells [22] and has been rarely explored in applications associated with electroanalytic [23]. To improve the electrochemical properties of electrodes it is necessary to modify the electrode surface. Surface modifications play a role as a catalyst and/or to increase the electroactive area, improving the sensitivity in electroanalytical applications [24]. There is a wide variety of nanomaterials used in the modification of electrode surfaces, as transition metal oxides, such as NiO [25], $Co_3O_4$ [26], CuO [27], $Fe_2O_3$ [28] among others. These oxides can be synthesized by various techniques

where it is possible to adjust the morphology and obtain a nanoscale size [29]. Hematite (α-$Fe_2O_3$) is a stable and cost-effective iron oxide with semiconductor properties, making it one of the most promising materials [30]. It is widely used in catalysis, electrochemical and gas sensors, photocatalysis, and electrocatalysis [31-33]. Iron oxide materials at the nanometer scale are particularly valuable for electrochemical sensors, offering excellent stability and durability for detecting pharmaceutical substances and identifying toxic health hazards in various media [34].

On the other hand, computer simulations are a valuable tool to study the interaction between molecules and surfaces, to aid in the design of electrochemical sensors. Models range from detailed and time-consuming molecular dynamics simulations [35], to approximate and faster implicit solvent approaches [36], [37] that use continuum dielectric theory. One popular implicit model is the Poisson-Boltzmann equation, which is used in the present study.

In this work the surface modification of a carbon paper electrode with α-$Fe_2O_3$ (hematite) nanoparticles for the voltammetric determination of atropine in beverages was performed. This study is the first to explore the electrochemical behavior of carbon paper with hematite for atropine detection. Based on the results obtained in this study, it is highlighted that from the properties of both materials, hematite and CP, enable the development of a simple, economical electrode with high potential for portable, miniaturizable, and disposable electroanalysis applications, specifically for in-situ detection of chemical submission drugs.

## 2. Methodology

### Reagents and Materials

All reagents used were of analytical grade. These included orthophosphoric acid ($H_3PO_4$, 85%), boric acid ($H_3PO_4$), glacial acetic acid ($CH_3COOH$), sodium hydroxide (NaOH), ferrous nitrate nonahydrate ($Fe(NO_3)_3 \times 3H_2O$), potassium ferrocyanide trihydrate ($K_4[Fe(CN)_6]3H_2O$), potassium ferricyanide trihydrate ($K_3[Fe(CN)_6]3H_2O$), Nafion® 5% and isopropanol (2-propanol) and atropine standard, which were obtained from Merck (Darmstadt, Germany). A high-pressure hydrothermal reactor was used for the synthesis of nanoparticles. A 3-electrode cell was used where the working electrode used was a carbon paper (sigracet 28 BC from FullCell Store) which consists of a macroporous layer of carbon fibers and a microporous layer of carbon black on top of it. The dimensions of the paper were

1.5 cm long and 0.5 cm wide. An Ag/AgCl (KCl sat.) electrode and a Pt wire counter electrode were used as reference electrode. Cyclic voltammetry (CV) and square wave voltammetry (SWV) experiments were performed with a MultiEmStat4 HR PalmSens potentiostat. Microscopic analyses were performed through transmission electron microscope (TEM) used at 120 Kv (high resolution TEM Hitachi HT7700, chiyoda, Tokyo, Japan), field emission scanning electron microscope (FESEM) Zeiss SUPRA TM 40 with Gemini column and Schottky field emission tip (tungsten at 1800 K). Chemical composition analysis was performed using a Shimadzu 6000 X-ray diffractometer (XRD) Shimadzu 6000 X-ray diffractometer (Nakagyo, Kyoto, Japan) (Cu-Ka radiation, 40 kV and 30 mA). The scanning was performed at room temperature using 2θ ranging from 20° to 70°.

**Synthesis of $Fe_2O_3$ nanoparticles**

$Fe_2O_3$ nanoparticles were synthesized following the methodology proposed by Liu J et al [38]. For this purpose 3.8779 g of $Fe(NO_3)_3 \times 3H_2O$ was added in a beaker and dissolved in 16 mL of ultrapure water and stirred until the salt was completely dissolved. In another beaker 0.1920 g NaOH was added and dissolved in 16 mL ultrapure water. The NaOH solution was added dropwise over the $Fe(NO_3)_3 \times 3H_2O$ solution while maintaining constant stirring. Once all the NaOH was added, the solution was stirred for 15 min and then taken to a hydrothermal reactor, which was placed in an oven at 200°C for 5 h. After this time, the product was allowed to cool to room temperature and then washed with ultrapure water and centrifuged for 10 min. This was repeated 6 times, where the last wash was performed with ethanol. Finally, a red precipitate was obtained, which was dried in an oven at 60°C for 3 h, then crushed in a mortar and stored in a desiccator.

**Modification and optimization of the working electrode**

**Preparation of the $Fe_2O_3$ ink**

This procedure consisted of the preparation of different $Fe_2O_3$ suspensions with different amounts of the oxide. Eight suspensions were prepared, each containing 0.50 mg, 0.75 mg, 1.00 mg, 1.25 mg, 1.50 mg, 2.50 mg, 3.00 mg and 5.00 mg, respectively, and 833 µL of ultrapure deionized water, 167 µL of isopropanol and 20 µL of Nafion. Finally, the ink was

placed in an ultrasonic bath for 30 min. Each time the electrode surface modification was performed, the sonication step was repeated to ensure that the suspension was homogeneous.

**Electrode Optimization and Modification**

The sigracet 28 BC paper was sized in 1.5 cm long by 0.5 cm wide portions (original dimensions were 10×10 cm). Then, the drop-casting methodology was followed, depositing a small amount of nanoparticles on a solid surface. When the solvent evaporates, the material is distributed uniformly forming a thin film. This technique has been used by several authors for the modification of electrodes [30-32]. A 25 µL aliquot of the prepared ink was added to each piece of paper and then placed in an oven at 80°C for 15 min

**Computational simulations**

The electrostatic component of the interaction free energy ($\Delta G_{int}$) between a carbon black (the conductive part of the CP) or $Fe_2O_3$ surface and atropine at different orientations was computed with the Poisson-Boltzmann solver PyGBe [42], [43], for different values of pH. Following a computational protocol used in previous work [44], the interaction free energy was assessed for all possible orientations of atropine with respect to the surface, where the orientation was characterized by the tilt angle ($\alpha_{tilt}$, from 0º to 180º) between atropine dipole moment and the surface's normal, and the rotation angle ($\alpha_{rot}$, from 0º to 360º), about the dipole moment vector. Also, using the interaction free energy, the probability of each orientation was calculated.

The molecular structure of atropine was extracted from the protein data bank (PDB) starting from the structure of phospholipase (PDB code 3OSH) [45], and parameterized (charge and radius) using Amber [46], [47] and Antechamber, with the semi-empirical model AM1-BCC [48]. Atropine can be found in protonated ($q_{net}$=+1e) and deprotonated (neutral) states, which were obtained with Avogadro [49]. The permittivity of atropine was set to $\epsilon_{atr}$ = 4, whereas the solvent (water) had $\epsilon_{solv}$ = 80 and with an inverse of the Debye length of $\kappa$ = 0.113 $Å^{-1}$, equivalent to solution with 0.12 M of NaCl.

The surface was modeled with a constant charge density. Starting from the zeta potential of carbon black and $Fe_2O_3$ at different [50], [51] , and assuming it is found one Debye length away from the surface [52] (although this is an open question [53]), the Debye-Huckel theory

was used to back-calculate an effective surface charge. The $Fe_2O_3$ nanoparticles were close to 50nm in diameter, which placed adsorbed atropine far from carbon black in the CB/ $Fe_2O_3$ surface. Hence, the CB/ $Fe_2O_3$ surface was characterized with the zeta potential of $Fe_2O_3$ only.

Further details of the numerical model and parameters can be found in section 2 in supplementary information.

## 3. Results and discussion

### Structural and morphological characterization of α-$Fe_2O_3$

The nanoparticles obtained from the hydrothermal synthesis were characterized by X-ray diffraction (XRD), Transmission Electron Microscopy (TEM) and Field Emission Scanning Electron Microscopy (FESEM). Figure 1 shows the diffractogram of the synthesized $Fe_2O_3$ nanoparticles, where the characteristic peaks correspond to the pure rhombohedral α–$Fe_2O_3$ phase (JCPDS No. 33-0664) [54], [55]. No impurity peaks are detected in the x-ray diffraction pattern, confirming that the synthesized products correspond to α–$Fe_2O_3$ free of impurities.

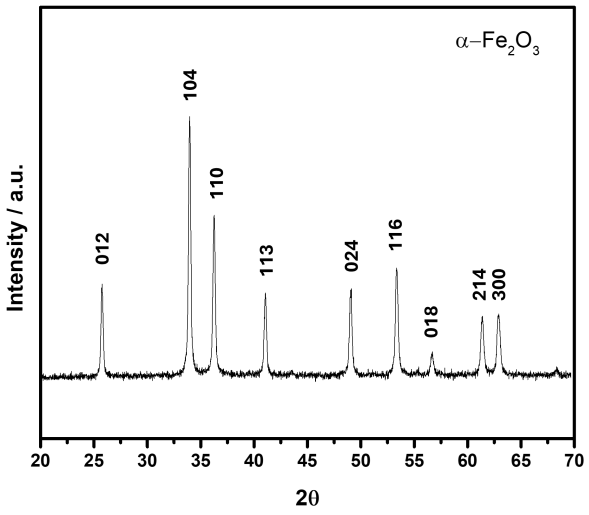


**Figure 1.** XRD pattern of α–$Fe_2O_3$ synthesized hydrothermally.

To analyze the morphology of the synthesized oxide α–$Fe_2O_3$, characterizations were performed by FESEM (see Fig.2 (a-b) and TEM (see Fig. 2c). The images obtained by FESEM reveal that the material presents a spherical and, in general, homogeneous morphology. On the other hand, the images obtained by TEM (Fig. 2c) corroborate the morphology observed by FESEM and, in addition, allow identifying that some of the nanoparticles of α–$Fe_2O_3$ present a more cubic morphology, although these occur less frequently compared to the spherical particles. Figure 2d shows the histogram of the size distribution obtained from the statistical analysis of 83 particles. The size distribution was well-fitted to a Gaussian curve, with an average length of 55.8 nm and a standard deviation of 14.2 nm. The observed morphologies are typical for $Fe_2O_3$ synthesized using the methodology described in this work [33-35]. The size of the synthesized $Fe_2O_3$ nanostructure offers significant advantages as an electrode material, primarily due to its large surface area.

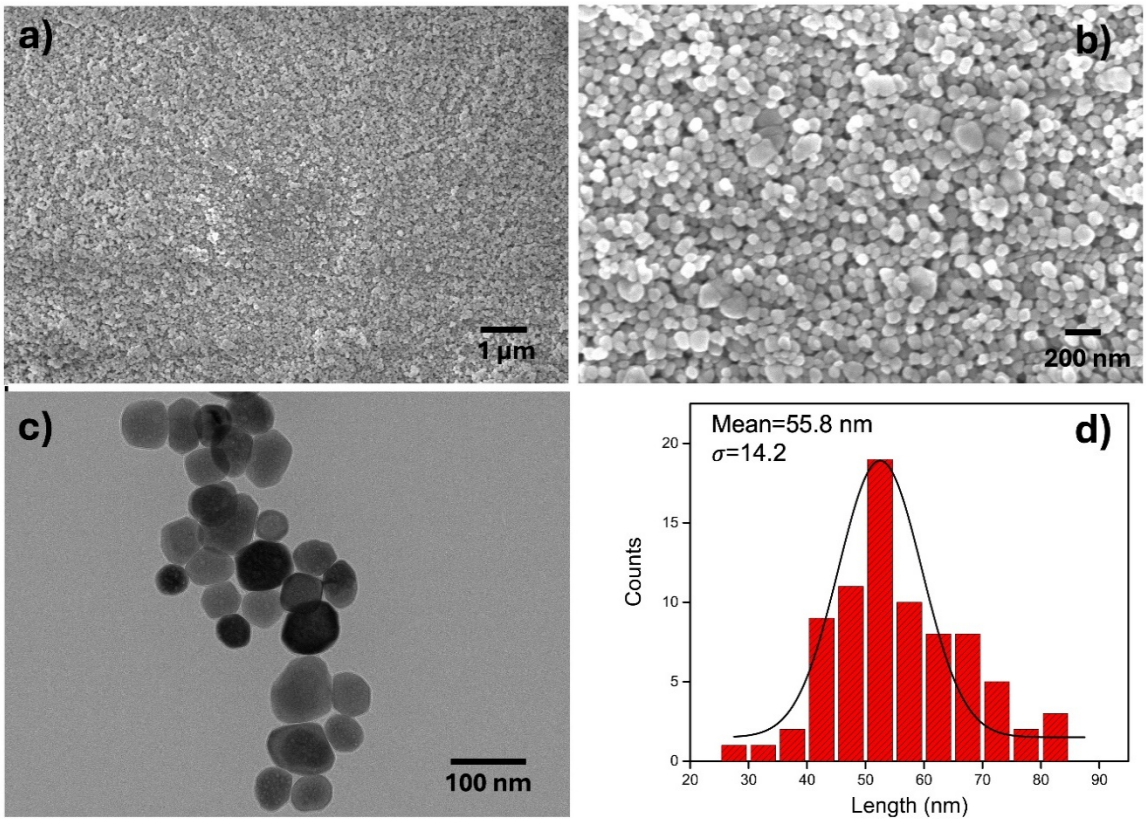


**Figure 2.** FESEM images of a- $Fe_2O_3$ synthesized at different magnifications; 25kX (a) and 100kX (b). TEM images 50kX (c) and histogram (d).

After characterizing and confirming that the nanoparticles obtained from the hydrothermal synthesis corresponded to $Fe_2O_3$, they were used to modify the surface of the CP electrode.

**Morphological characterization of the electrode surface**

To analyze the surface of the carbon paper (CP) before and after being modified with $Fe_2O_3$ nanoparticles, morphological characterizations were performed by FESEM, obtaining the images shown in Figures 3 (a-d).

The images obtained by FESEM at different magnifications for the CP can be seen in Figure 3 (a-b) and reveal a dense and homogeneous surface composed of uniformly distributed carbon black particles. These particles present a spherical morphology, forming small agglomerates, which is characteristic of this nanomaterial [57].

Figure 3 (c-d) shows the images obtained for CP modified with $Fe_2O_3$ at different magnifications. These images corroborate the modification of the electrode surface since the same morphology of the nanoparticles presented in Figure 2b is observed. The nanoparticles are uniformly distributed on the paper surface, forming agglomerations in certain sectors. This uniform distribution indicates a good dispersion of the iron oxide nanoparticles on the CP surface. From FESEM images obtained for the characterization of the CP and CP/$Fe_2O_3$ electrode, the difference in the surface morphology between the electrode before and after the addition of the iron oxide nanoparticles is observed, highlighting the presence of particles and structures that indicate the modification on the electrode surface.

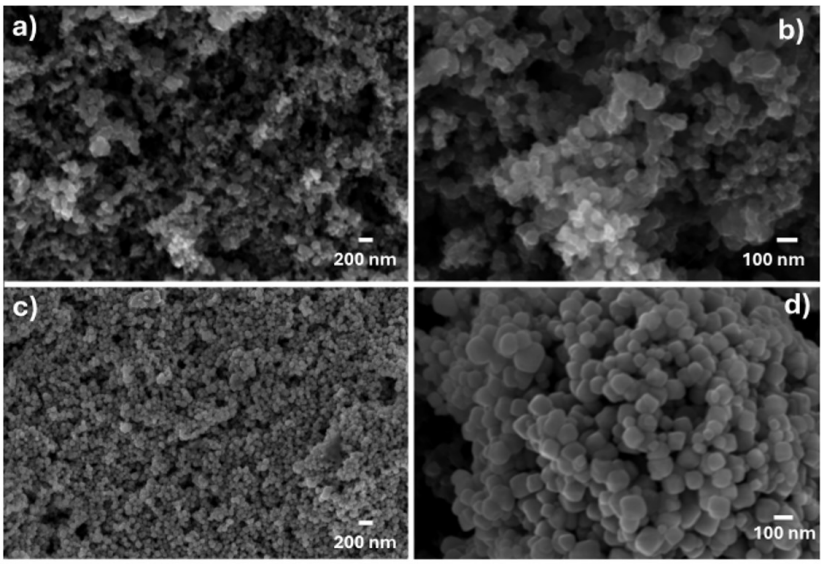


**Figure 3.** FESEM images of the surface of the unmodified (a-b) and $Fe_2O_3$-modified (c-d) paper electrode at different magnifications; 50kX(a-c) and 150kX(b-d).

### Electrochemical Characterization of Electrodes

To assess the electrochemical characteristics of the unmodified and modified electrodes, they were characterized using cyclic voltammetry in an aqueous solution of 0.01 M ferri/ferrocyanide $[Fe(CN)_6]^{3-}/[Fe(CN)_6]^{4-}$ containing 0.1 M KCl. Figure 4 depicts a comparison between voltammograms obtained using CP and CP/$Fe_2O_3$ electrode. The image shows that in the case of the CP electrode, the peaks are very wide and unresolved. However, modifying the CP electrode with $Fe_2O_3$ significantly improves its electrochemical activity, displaying high current peaks more reversible compared to the CP electrode. This combination increased the electroactive surface area and improving overall performance [57-59]. The oxidation and reduction peak potentials obtained with the CP/$Fe_2O_3$ electrode are 0.347 V and 0.101 V, respectively [61]. The oxidation and reduction peak currents for the modified electrode are 0.942 and -0.948 µA respectively, being significantly higher compared to the unmodified electrode, which can be observed in Figure 4. This increase in peak currents indicates a higher density of active sites available for electrochemical reaction on the CP/$Fe_2O_3$. The presence of $Fe_2O_3$ nanoparticles increases the conductivity of the material, providing a larger effective surface area of the electrode [62].

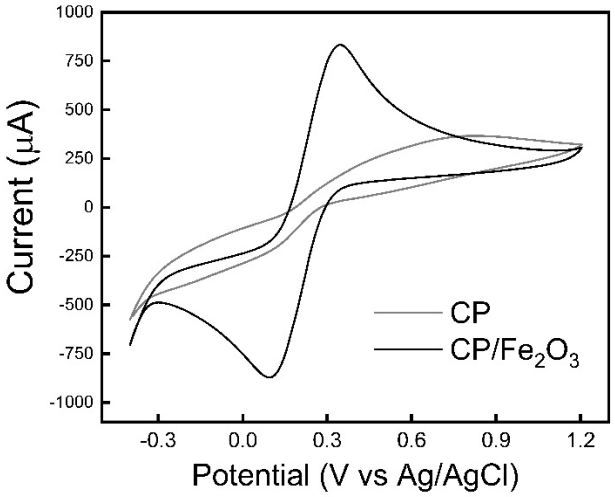


**Figure 4**. Cyclic voltammogram of 0.01 mol $L^{-1}$ $[Fe(CN)_6]^{3-}$/ $[Fe(CN)_6]^{4-}$ using CP (gray line) and CP/$Fe_2O_3$ (black line) in 0.1 mol $L^{-1}$ KCl (Blank). Scan rate: 0.10 V $s^{-1}$.

**Electrochemical behavior of Atropine**

To know the electrochemical response of atropine, a study was carried out using a highly sensitive electrochemical technique such as SWV.

Figure 5 shows the square wave voltammogram (SWV) obtained for the response of 1.10 mM Atropine using CP (gray line) and CP/$Fe_2O_3$ (black line). The current recorded using the CP electrode was 81 μA, while for the CP/$Fe_2O_3$ electrode it was 101 μA. This difference in current indicates a better sensitivity of the modified electrode [57], [63].

The improved electrochemical response of the modified electrode can be explained by several reasons. First, the presence of $Fe_2O_3$ can facilitate the electron transfer between atropine and the electrode, leading to a higher measured current [64], due to the conductive properties of iron oxide, which can act as a redox mediator, facilitating the electron transfer between atropine and the electrode. This occurs because $Fe_2O_3$ has a crystalline structure that allows good enough electrical conductivity and a high density of surface-active sites, which can adsorb atropine molecules more efficiently [65]. The CP/$Fe_2O_3$ electrode demonstrates

an improvement in current response compared to the unmodified electrode when detecting the same concentration of atropine.

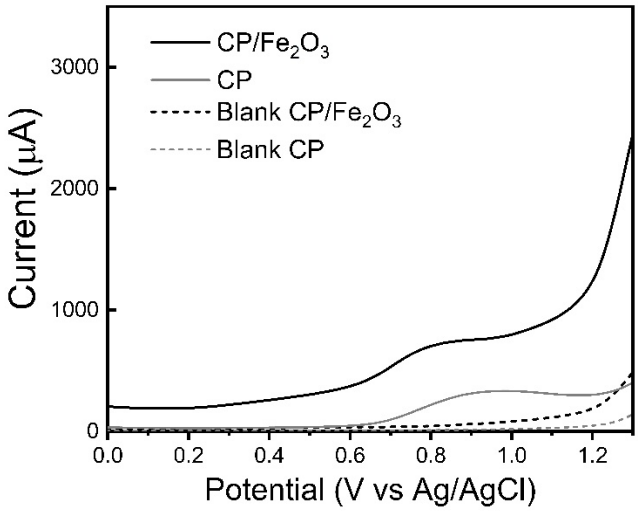


**Figure 5.** Voltammetric response for 1.10 mM atropine using CP (gray line) and CP/$Fe_2O_3$ (black line) using 0.10 M Britton-Robinson buffer pH 11.5.

**Optimization of chemical and electrochemical variables for the determination of Atropine**

To carry out the analytical methodology, the effect of chemical and electrochemical variables (effect of pH and amount of modifying agent) on the voltammetric response of a known concentration of Atropine was evaluated.

**Optimization of pH**

The effect of pH on the voltammetric response of atropine was evaluated over a pH range of 2.0 - 12.0 using Britton-Robinson (BR) buffer using CP and CP/ $Fe_2O_3$ electrode (Figure 6) (the relationship between potential and pH is presented in Figure S1). Data obtained using both electrodes indicate an absence of signal between pH 2.0 - 6.0, while increasing currents are recorded in the pH range 8.0 - 12.0. Both electrodes exhibited a similar behavior in general terms with respect to the effect of pH, registering a maximum current at pH 11.5, so this pH was chosen to perform the subsequent analyses using both electrodes. This

observation is further supported by Poisson-Boltzmann calculations detailed next, highlighting the role of electrostatics in the pH shift.

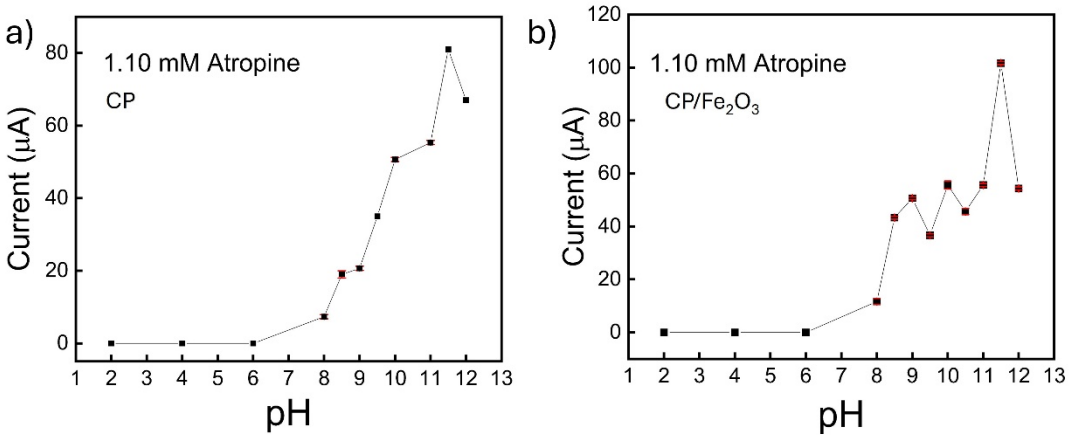


**Figure 6.** Study of the pH effect of the 1.10 mM atropine response using CP and CP/$Fe_2O_3$ in 0.1 M Britton-Robinson buffer by square wave voltammetry (SWV). (a-b) Current versus pH dependence.

**Simulations of Atropine adsorbing on CB and CB/$Fe_2O_3$ surface.**

For the realization of these calculations, it was used as a carbon paper model (CP), only carbon black (CB), which completely covers it and is the surface that is in contact with atropine. In the case of the electrode modified with hematite (CP/$Fe_2O_3$), the surface that was considered for this simulation was only hematite, since it is the surface that detects atropine, and it is labelled as CB/$Fe_2O_3$. The Poisson-Boltzmann calculations of the interaction of atropine with CB and CB/$Fe_2O_3$ surfaces are summarized by Figure 7. This image shows a repulsive interaction (positive $\Delta G_{int}$) for low pH, which becomes attractive as pH increases. This effect is more pronounced for CB surface, which starts being electrostatically favorable at pH 6, whereas with CB/$Fe_2O_3$ this happens at around pH 10, both in with atropine in protonated state. The reason why the interaction is inverted is evident from the dotted lines in Figure 7, which represent the imposed surface charge on the CB and CB/$Fe_2O_3$ surfaces, computed from the zeta potentials. For low pH, the surface charge is positive, repelling the positively charged protonated atropine, however, the opposite occurs for high pH, where surface charge becomes negative. The cross-over pH where the surface charge inverts was

around 6 for CB surface and 9 for the CB/$Fe_2O_3$ surface. On the other hand, for atropine in deprotonated state the electrostatic interaction is low. The peak in pH 11 in Figure 6, indicating a higher presence of adsorbed atropine, is somewhat surprising considering atropine pKa is 9.43, and the less attractive deprotonated state should be more likely. For this to make sense, the atropine-surface interaction needs to be increasingly favorable beyond the nominal pKa, such that the protonated atropine prevails. This demonstrates that the surface is imposing a shift in pKa, giving a higher probability to find atropine in a protonated state at pH higher than 9.43. Beyond pH 11, most atropines are deprotonated, explaining the current decrease for pH 12 in Figure 6. This pKa shift is usually known as charge regulation [66].

The higher currents throughout pH reported in Figure 6 for the $Fe_2O_3$-modified surface cannot be explained by electrostatics and is probably a result of non-polar interactions. For pH higher than 8 and lower than 11, the zeta potential of $Fe_2O_3$ is closer to zero than carbon black [67], [68] , and hence, is less charged (as depicted by Figure 7) and more hydrophobic. Molecule-surface hydrophobic interactions in water are favorable [69], explaining the enhanced signal in Figure 6b compared to Figure 6a in that pH range. According to these results, which indicate on the one hand a prevalence of atropine protonated at pH 11.5 due to the effect of the surface and a negative surface that generates strong electrostatic interactions, the best sensitivity of the method to pH 11.5 described in Fig. 6 is explained.

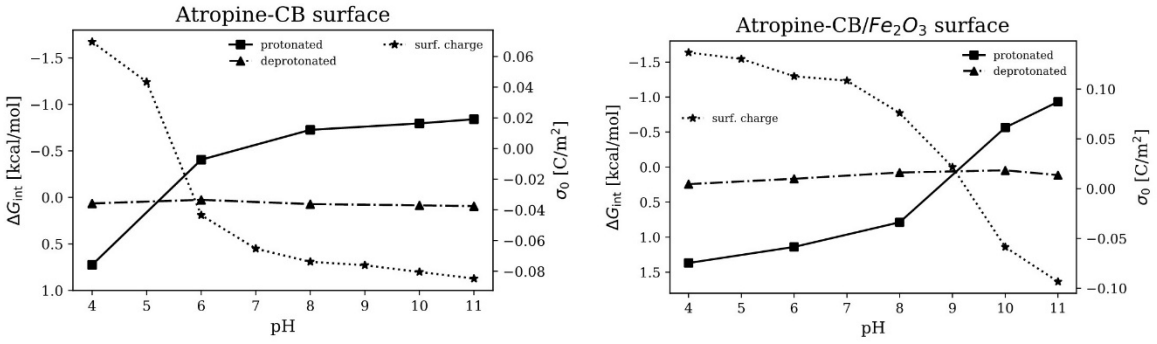


**Figure 7.** Electrostatic component of the interaction free energy ($\Delta G_{int}$) of atropine with a CB (left) and CB/$Fe_2O_3$ (right) surface, which becomes increasingly attractive (negative) with pH. The dotted lines correspond to the surface charge in each case computed from the zeta potential, also becoming negative with increasing pH.

## Optimization of the modifying agent

The effect of the amount of $Fe_2O_3$ on the electrochemical response of 1.29 mM atropine was studied by preparing 8 suspensions with different amounts of the nanoparticles between 0.50 and 5.00 mg dissolved on 833 µL of ultrapure deionized water, 167 µL of isopropanol and 20 µL of Nafion. 25 µL of these suspensions were then deposited on the CP surface. Figure 4S shows that the amount of $Fe_2O_3$ has a significant effect on the current response obtained for 1.29 mM atropine. It is observed that the electrode modified with the suspension containing 1 mg/mL of $Fe_2O_3$ provided the best electrochemical response, where the maximum current peak is observed. This behavior suggests that at this amount of modifying agent an optimal interaction between the modified electrode and atropine is achieved, which is possibly due to an improvement in the available active surface and a facilitation of the redox process. However, by increasing the amount of $Fe_2O_3$ in the suspension above 1.00 mg, a decrease in current was observed, which could be attributed to an excess of $Fe_2O_3$ on the electrode surface, reducing the area available for the electrochemical reaction of atropine. In addition, at high amounts, $Fe_2O_3$ particles can form agglomerations, decreasing the effectiveness of the interaction between the electrode surface and atropine.

Based on these results it was determined that the appropriate amount of $Fe_2O_3$ to use to modify the electrodes for atropine detection was 1.0 mg of $Fe_2O_3$ in the suspension, therefore, that was the amount of modifying agent used to perform the subsequent studies.

## Calibration curve

For comparison, calibration curves were performed for atropine determination using the CP and CP/$Fe_2O_3$ electrode. Figure 8 shows (a) voltammograms and (b) calibration curve using CP. A linearity range of 0.38 to 2.35 mM was obtained, with an equation y = 116.29x - 37.33 and a correlation coefficient of 0.998. The limit of detection (LD) was calculated as $LD = 3S_a/b$ [70], where $S_a$ is the standard deviation of the intercept and b the slope of the calibration curve, obtaining a value of 0.090 mM; and the limit of quantification was calculated as $LQ = 10S_a/b$, corresponding to 0.301 mM, while (c) shows the square wave voltammograms and

(d) the calibration curve for atropine obtained with the CP/$Fe_2O_3$ electrode, obtaining a linear range from 0.26 to 2.64 mM with an equation y = 116.37x - 11.24 and a correlation coefficient of 0.999. The LD obtained was 0.075 mM and the LQ was 0.250 mM.

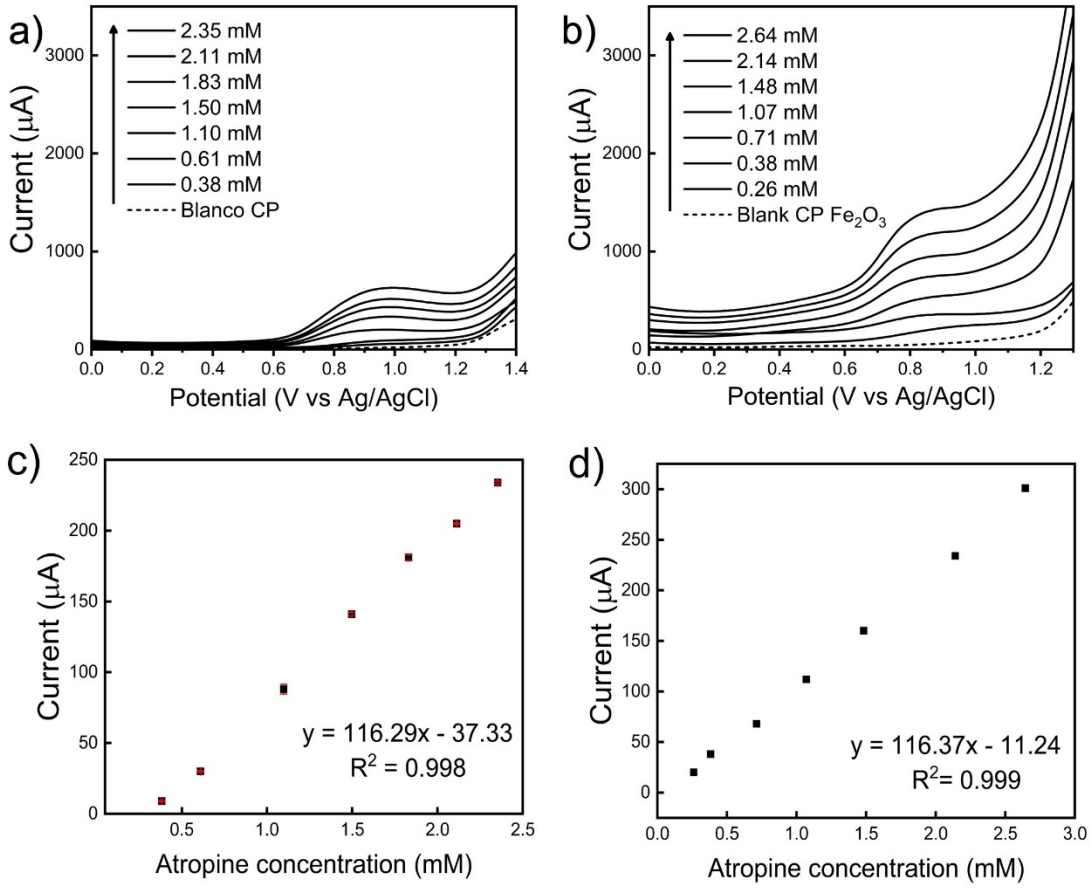


**Figure 8.** (a-b) SWV voltammograms and (c-d) calibration curve for atropine using CP and CP/ $Fe_2O_3$ in 0.10 M Britton-Robinson Buffer pH 11.5.

Comparison of the responses of both systems showed that the CP/$Fe_2O_3$ electrode yielded lower LD and LQ. In addition, both electrodes show high correlation coefficients, 0.998 for CP and 0.999 for CP/$Fe_2O_3$, indicating a good relationship between atropine concentration and measured response.

## Repeatability study

To evaluate the repeatability of the modified and unmodified electrode, a study was performed by making eight individual current measurements using a single electrode. The results obtained with a CP and CP/$Fe_2O_3$ are shown in Figure 5S, where no significant statistical difference between the recorded currents is observed which indicates excellent repeatability in the current measurements.

## Study in real samples

It has been reported in the literature that the average lethal dose of atropine for an adult person is 100 mg [70], [71]. Considering that a person consumes approximately 250 mL of beverage per glass, the lethal concentration of atropine in such a glass would be around~1.38 mM. Therefore, the dose used to dope a person is lower than that value, making accurate detection of atropine at lower concentrations crucial. To minimize the influence of possible interferents on the measurement such as ethanol, the standard addition method was employed. Measurements were carried out on Gin samples spiked with a known concentration of 0.21 mM of atropine at a ratio of 1:100 in BR buffer pH 11.5. Each analysis was measured in triplicate (n =3).

Figure 6S (a-b) shows the voltammetric responses obtained with the CP electrode for different atropine concentrations, where a proportional increase of the peak current with increasing concentration is observed, which can be confirmed with the linear regression equation constructed, $y = 171.76x + 22.39$; $R^2 = 0.993$. Extrapolating that equation, it was obtained that the concentration of atropine present in the sample was 0.13 ± 1.9% mM. However, the sample had been previously fortified with 0.21 mM atropine, obtaining a recovery percentage of 62%, which indicates that the CP electrode, despite presenting good linearity, is affected by possible interferents present in the sample, such as alcohol, phenolic compounds, among others.

The responses obtained with the modified electrode are shown in Figure 6S (c-d), where the peak currents recorded are higher compared to those obtained with the unmodified electrode. From the graph Current v.s Concentration the following equation was obtained: $y = 259.92 + 51.71$; $R^2 = 0.989$, from which it was possible to determine the concentration of atropine present in the sample, 0.20 ± 0.9% mM. A recovery percentage of 95% was obtained, indicating that the presence of interferents does not affect the detection of atropine by the CP/$Fe_2O_3$ electrode. This recovery percentage coincides with that reported in the literature, where different authors obtained recovery percentages between 100 and 120 % [72], [73].

Comparing the results obtained with both electrodes, it can be seen that the CP/$Fe_2O_3$ electrode presents a superior performance in the detection of atropine in gin, with a recovery percentage of 95% compared to the 62% obtained with the CP electrode. This indicates that, although both electrodes are capable of detecting atropine in a complex sample such as gin, the CP/$Fe_2O_3$ electrode allows more precise quantification of the concentration of this alkaloid in the beverage, which may be related to its selectivity to the analyte under study, which minimizes the effect on the current response of the components of gin.

## 4. Conclusions

Based on the results obtained in this study for the detection of atropine, the incorporation of $\alpha$-$Fe_2O_3$ on a carbon paper electrode led to an improvement in the electrochemical activity of the electrode, which is reflected in the increase in the current measured when detecting atropine compared to the unmodified electrode. Morphological characterization by FESEM showed a uniform distribution of $Fe_2O_3$ nanoparticles on the CP surface, indicating that the drop-casting process achieved a homogeneous dispersion and adequate adhesion of the modifying agent, which is crucial to facilitate a larger active surface area for the atropine oxidation reaction on the electrode. Thus, the improvement in the electrochemical activity of the CP/$Fe_2O_3$ electrode can be attributed to this uniform distribution of the nanoparticles, which optimizes the electrochemical interaction between the analyte and the electrode. This result is consistent with the strong effect of the amount of modifying agent required for proper atropine detection. Also, the optimization of pH was

relevant to maximize the efficiency of the modified electrode. The evaluation of the pH effect showed that pH has a large effect on the current response for atropine. At low pH no significant response was obtained, however, the response increased with pH, peaking at pH 11.5. The pH dependent behavior can be explained with electrostatic simulations that imply that, at high pH, protonated atropine had a more attractive interaction with the surfaces, compared with its deprotonated counterpart, as the effective surface charge was negative. Considering that the pKa of atropine is 9.4, the peak in pH 11.5 indicates that the surface induces a shift in pKa, making the protonated state prevalent at a pH higher than the regular pKa. The optimization of the modifying agent determined that the optimal amount of $Fe_2O_3$ was 1 mg/mL. Higher amounts of $Fe_2O_3$ generate a decrease in the electrochemical efficiency, possibly due to the formation of agglomerates of the nanomaterial, which limits the accessibility of the electroactive species. From the calibration curves constructed it could be determined that the LOD and LQ recorded using the CP/$Fe_2O_3$ electrode were lower compared to the unmodified electrode (LOD = 0.075 mM and LQ = 0.250 mM for CP/$Fe_2O_3$ and for CP, LOD = 0.096 mM and LQ = 0.320 mM), which evidences a better ability to detect lower concentrations of atropine with high precision and linearity by CP/$Fe_2O_3$. Regarding the repeatability of the electrodes, the results obtained with the CP electrode showed a mean current of 82.9 µA and a relative standard deviation (RSD) of 1.37%, indicating excellent repeatability in the current measurements. Similarly, the CP/$Fe_2O_3$ electrode presented a mean current of 100.9 µA and RSD of 1.08%, also corroborating a high repeatability in the measurements. Both electrodes showed high accuracy and reliability in the detection of atropine.

Finally, in the case of real samples, the effect of interferents makes quantification difficult using CP, but not detection, achieving reproducible results and within the limits in which atropine can cause chemical submission effects in a person. On the other hand, the CP/$Fe_2O_3$ electrode not only showed a higher peak current and good linearity ($R^2$ = 0.989), but also a better recovery, which was 95%, indicating that the presence of interferents did not significantly affect the detection of atropine.

## Declaration of Competing Interest

The authors declare that they have no known competing financial interests or personal relationships that could have appeared to influence the work reported in this paper.

## Acknowledgments

This work was funded by the National Agency for Research and Development (ANID) through Millennium Institute on Green Ammonia as Energy Vector MIGA, ANID/Millennium Science Initiative Program/ICN2021_023(MJA); Subvención a Instalación en la Academia (2021), (2022); (SIA85220089-SIA77210080), FONDECYT INICIACION 11230219, EQM190016, ANID BECA DOCTORADO NACIONAL Nº21220363 - Nº 21241181 and CCTVal through ANID PIA/APOYO AFB220004.

## 5. References

[1] "Sumisión química | Comunidad de Madrid." Accessed: Jun. 27, 2023. [Online]. Available: https://www.comunidad.madrid/servicios/salud/sumision-quimica

[2] S. Djezzar, F. Questel, E. Burin, and S. Dally, "Chemical submission: Results of 4-year French inquiry," *Int J Legal Med*, vol. 123, no. 3, pp. 213–219, May 2009, doi: 10.1007/s00414-008-0291-x.

[3] E. Profesional De Psicología, "Las benzodiacepinas y sus efectos sobre la ansiedad Benzodiazepines and their effects on anxiety Maité Díaz-Peñaloza* Este es un artículo Open Access bajo la licencia Creative Commons Atribución-NoComercial-CompartirIgual 4.0," vol. 31, pp. 169–180, 2017, doi: 10.24265/cultura.2017.v31.09.

[4] F. Hoffmann, "Benefits and risks of benzodiazepines and Z-drugs: Comparison of perceptions of GPs and community pharmacists in Germany," *GMS German Medical Science*, vol. 11, Jul. 2013, doi: 10.3205/000178.

[5] "Drogas de sumisión química: efectos, usos y prevención." Accessed: Nov. 01, 2022. [Online]. Available: https://cuidateplus.marca.com/bienestar/2022/03/13/drogas-sumision-quimica-efectos-usos-prevencion-179623.html

[6] "Rang y Dale : farmacologia - Universidad de Chile." Accessed: Oct. 21, 2023. [Online]. Available: https://bibliotecadigital.uchile.cl/discovery/fulldisplay/alma991005927609703936/56UDC_INST:56UDC_INST

[7] "Museu da Farmacia." Accessed: Nov. 01, 2022. [Online]. Available: https://www.museudafarmacia.pt/detalhe.aspx?lang=sp&area=storymap&f=87&bid=68

[8] "Formulario Nacional de Medicamentos. CUBA. - ATROPINA." Accessed: Nov. 01, 2022. [Online]. Available: http://fnmedicamentos.sld.cu/index.php?P=FullRecord&ID=115

[9] "AHFS drug information 2012 | WorldCat.org." Accessed: Nov. 01, 2022. [Online]. Available: https://www.worldcat.org/es/title/ahfs-drug-information-2012/oclc/774043698

[10] P. H. Hinderling, U. Gundert-Remy, and O. Schmidlin, "Integrated Pharmacokinetics and Pharmacodynamics of Atropine in Healthy Humans I: Pharmacokinetics," *J Pharm Sci*, vol. 74, no. 7, pp. 703–710, Jul. 1985, doi: 10.1002/JPS.2600740702.

[11] M. J. Van Der Meer, H. K. L. Hundt, and F. O. Müller, "The metabolism or atropine in man," *Journal of Pharmacy and Pharmacology*, vol. 38, no. 10, pp. 781–784, Oct. 1986, doi: 10.1111/J.2042-7158.1986.TB04494.X.

[12] "Determinación de atropina sulfato y difenoxilato clorhidrato en reasec tabletas.: Validación." Accessed: Nov. 02, 2023. [Online]. Available: http://scielo.sld.cu/scielo.php?pid=S0034-75152001000200003&script=sci_arttext&tlng=pt

[13] C. García-Caballero, A. Cruz-Landeira, and Ó. Quintela-Jorge, "Sumisión química en casos de presuntos delitos contra la libertad sexual analizados en el Instituto Nacional de Toxicología y Ciencias Forenses (Departamento de Madrid) durante los años 2010, 2011 y 2012," *Revista Española de Medicina Legal*, vol. 40, no. 1, pp. 11–18, Jan. 2014, doi: 10.1016/J.REML.2013.07.003.

[14] P. Medicinales Aromáticas, "Boletín Latinoamericano y del Caribe de," *Plantas Medicinales y Aromáticas*, vol. 6, no. 6, 2007, Accessed: Nov. 02, 2023. [Online]. Available: http://www.redalyc.org/articulo.oa?id=85617472032

[15] E. Stashenko and J. René Martínez, "GC-MS GC-MS: herramienta fundamental para el análisis de drogas de uso ilícito," *Scientia Chromatographica*, vol. 4, no. 1, pp. 21–33, 2012, doi: 10.4322/sc.2012.003.

[16] J. Gañán, G. Martínez-García, S. Morante-Zarcero, D. Pérez-Quintanilla, and I. Sierra, "Nanomaterials-modified electrochemical sensors for sensitive determination of alkaloids: Recent trends in the application to biological, pharmaceutical and agri-food samples," *Microchemical Journal*, vol. 184, p. 108136, Jan. 2023, doi: 10.1016/J.MICROC.2022.108136.

[17] D. Y. Reasco-Pincay and M. I. Márquez-Alcívar, “Determinación de paracetamol en un agua residual simulada mediante voltamperometría de onda cuadrada usando un electrodo de carbón vítreo dopado con disco de platino,” *Ibero-American Journal of Engineering & Technology Studies*, vol. 3, no. 1, pp. 238–255, Apr. 2023, doi: 10.56183/IBEROTECS.V3I1.599.

[18] A. La Rosa-Toro G *et al.*, “Estudio electroquímico de la remoción de los Iones Cd(II) en soluciones acuosas mediante carbón activado obtenido de la cáscara de naranja,” *Revista de la Sociedad Química del Perú*, vol. 88, no. 2, pp. 155–164, Aug. 2022, doi: 10.37761/RSQP.V88I2.387.

[19] “SIGRACET® Fuel Cell Components | SGL Carbon.” Accessed: Oct. 30, 2023. [Online]. Available: https://www.sglcarbon.com/en/markets-solutions/material/sigracet-fuel-cell-components/

[20] Á. Torrinha, M. Martins, M. Tavares, C. Delerue-Matos, and S. Morais, “Carbon paper as a promising sensing material: Characterization and electroanalysis of ketoprofen in wastewater and fish,” *Talanta*, vol. 226, May 2021, doi: 10.1016/j.talanta.2021.122111.

[21] J. Zeng, J. R. Nair, C. Francia, S. Bodoardo, and N. Penazzi, “Aprotic Li-O2 cells: Gas diffusion layer (GDL) as catalyst free cathode and tetraglyme/LiClO4 as electrolyte,” *Solid State Ion*, vol. 262, pp. 160–164, Sep. 2014, doi: 10.1016/J.SSI.2013.09.032.

[22] H. Guo *et al.*, “Gas Diffusion Layer for Proton Exchange Membrane Fuel Cells: A Review,” *Materials 2022, Vol. 15, Page 8800*, vol. 15, no. 24, p. 8800, Dec. 2022, doi: 10.3390/MA15248800.

[23] Á. Torrinha and S. Morais, “Electrochemical (bio)sensors based on carbon cloth and carbon paper: An overview,” *TrAC Trends in Analytical Chemistry*, vol. 142, p. 116324, Sep. 2021, doi: 10.1016/J.TRAC.2021.116324.

[24] C. Ximena *et al.*, “Estudio electroquímico de la preparación de electrodos modificados para diferentes aplicaciones de energía y biológica”.

[25] T. Tavana and A. R. Rezvani, “Monitoring of atropine anticholinergic drug using voltammetric sensor amplified with NiO@Pt/SWCNTs and ionic liquid,” *Chemosphere*, vol. 289, p. 133114, Feb. 2022, doi: 10.1016/J.CHEMOSPHERE.2021.133114.

[26] H. Bagheri, S. M. Arab, H. Khoshsafar, and A. Afkhami, “A novel sensor for sensitive determination of atropine based on a Co3O4-reduced graphene oxide modified carbon paste electrode,” *New Journal of Chemistry*, vol. 39, no. 5, pp. 3875–3881, May 2015, doi: 10.1039/C5NJ00133A.

[27] Z. M. Khoshhesab, "Simultaneous electrochemical determination of acetaminophen, caffeine and ascorbic acid using a new electrochemical sensor based on CuO–graphene nanocomposite," *RSC Adv*, vol. 5, no. 115, pp. 95140–95148, Nov. 2015, doi: 10.1039/C5RA14138A.

[28] M. M. Vinay and Y. Arthoba Nayaka, "Iron oxide (Fe2O3) nanoparticles modified carbon paste electrode as an advanced material for electrochemical investigation of paracetamol and dopamine," *Journal of Science: Advanced Materials and Devices*, vol. 4, no. 3, pp. 442–450, Sep. 2019, doi: 10.1016/J.JSAMD.2019.07.006.

[29] S. Kumar, M. Kumar, and A. Singh, "Synthesis and characterization of iron oxide nanoparticles (Fe2O3, Fe3O4): a brief review," *Contemp Phys*, Jul. 2021, doi: 10.1080/00107514.2022.2080910.

[30] K. Zangeneh Kamali, P. Alagarsamy, N. M. Huang, B. H. Ong, and H. N. Lim, "Hematite Nanoparticles-Modified Electrode Based Electrochemical Sensing Platform for Dopamine," *The Scientific World Journal*, vol. 2014, no. 1, p. 396135, Jan. 2014, doi: 10.1155/2014/396135.

[31] R. Revathy, T. Sajini, C. Augustine, and N. Joseph, "Iron-based magnetic nanomaterials: Sustainable approaches of synthesis and applications," *Results in Engineering*, vol. 18, p. 101114, Jun. 2023, doi: 10.1016/J.RINENG.2023.101114.

[32] M. A. Rashed, M. Faisal, S. A. Alsareii, M. Alsaiari, M. Jalalah, and F. A. Harraz, "Highly sensitive and selective electrochemical sensor for detecting imidacloprid pesticide using novel silver nanoparticles/mesoporous carbon/hematite ore ternary nanocomposite," *J Environ Chem Eng*, vol. 10, no. 5, p. 108364, Oct. 2022, doi: 10.1016/J.JECE.2022.108364.

[33] M. Mazloum-Ardakani, N. Sadri, and V. Eslami, "Detection of Dexamethasone Sodium Phosphate in Blood Plasma: Application of Hematite in Electrochemical Sensors," *Electroanalysis*, vol. 32, no. 6, pp. 1148–1154, Jun. 2020, doi: 10.1002/ELAN.201900498.

[34] M. Mazloum-Ardakani, N. Sadri, and V. Eslami, "Detection of Dexamethasone Sodium Phosphate in Blood Plasma: Application of Hematite in Electrochemical Sensors," *Electroanalysis*, vol. 32, no. 6, pp. 1148–1154, Jun. 2020, doi: 10.1002/ELAN.201900498.

[35] J. Himmelstrup and V. R. Jensen, "Enabling Molecular-Level Computational Description of Redox and Proton-Coupled Electron Transfer Reactions of Samarium Diiodide," *Journal of Physical Chemistry A*, vol. 127, no. 17, pp. 3796–3803, May 2023, doi: 10.1021/ACS.JPCA.3C00418/SUPPL_FILE/JP3C00418_SI_002.XYZ.

[36] C. D. Cooper, N. C. Clementi, and L. A. Barba, "Probing protein orientation near charged nanosurfaces for simulation-assisted biosensor design," *Journal of Chemical Physics*, vol. 143, no. 12, p. 124709, Sep. 2015, doi: 10.1063/1.4931113/14800046/124709_1_ACCEPTED_MANUSCRIPT.PDF.

[37] S. A. Urzúa, P. Y. Sauceda-Oloño, C. D. García, and C. D. Cooper, "Predicting the Orientation of Adsorbed Proteins Steered with Electric Fields Using a Simple Electrostatic Model," *Journal of Physical Chemistry B*, vol. 126, no. 28, pp. 5231–5240, Jul. 2022, doi: 10.1021/ACS.JPCB.2C03118/SUPPL_FILE/JP2C03118_SI_001.PDF.

[38] J. Liu, J. Wang, J. Sun, Y. Li, and F. Lu, "Hydrothermal synthesis and characterization of monodisperse α-Fe2O3 nanocubes," *Micro Nano Lett*, vol. 9, no. 10, pp. 746–749, Oct. 2014, doi: 10.1049/MNL.2014.0212.

[39] D. Talarico, F. Arduini, A. Amine, I. Cacciotti, D. Moscone, and G. Palleschi, "Screen-printed electrode modified with carbon black and chitosan: a novel platform for acetylcholinesterase biosensor development," *Anal Bioanal Chem*, vol. 408, no. 26, pp. 7299–7309, Oct. 2016, doi: 10.1007/S00216-016-9604-Y/METRICS.

[40] A. Sánchez-Calvo, E. Núñez-Bajo, M. T. Fernández-Abedul, M. C. Blanco-López, and A. Costa García, "Optimization and characterization of nanostructured paper-based electrodes," *Electrochim Acta*, vol. 265, pp. 717–725, Mar. 2018, doi: 10.1016/J.ELECTACTA.2018.01.179.

[41] G. Gotti, D. Evrard, K. Fajerwerg, and P. Gros, "Oxygen reduction reaction features in neutral media on glassy carbon electrode functionalized by chemically prepared gold nanoparticles," *Journal of Solid State Electrochemistry*, vol. 20, no. 6, pp. 1539–1550, Jun. 2016, doi: 10.1007/S10008-016-3159-X/METRICS.

[42] C. D. Cooper and L. A. Barba, "Poisson–Boltzmann model for protein–surface electrostatic interactions and grid-convergence study using the PyGBe code," *Comput Phys Commun*, vol. 202, pp. 23–32, May 2016, doi: 10.1016/J.CPC.2015.12.019.

[43] C. D. Cooper, J. P. Bardhan, and L. A. Barba, "A biomolecular electrostatics solver using Python, GPUs and boundary elements that can handle solvent-filled cavities and Stern layers," *Comput Phys Commun*, vol. 185, no. 3, pp. 720–729, Mar. 2014, doi: 10.1016/J.CPC.2013.10.028.

[44] C. D. Cooper, N. C. Clementi, and L. A. Barba, "Probing protein orientation near charged nanosurfaces for simulation-assisted biosensor design," *Journal of Chemical Physics*, vol. 143, no. 12, p. 124709, Sep. 2015, doi: 10.1063/1.4931113/14800046/124709_1_ACCEPTED_MANUSCRIPT.PDF.

[45] "RCSB PDB - 3OSH: Crystal Structure of The Complex of Group 1 Phospholipase A2 With Atropin At 1.5 A Resolution." Accessed: Oct. 01, 2024. [Online]. Available: https://www.rcsb.org/structure/3OSH

[46] J. Wang, R. M. Wolf, J. W. Caldwell, P. A. Kollman, and D. A. Case, "Development and testing of a general amber force field," *J Comput Chem*, vol. 25, no. 9, pp. 1157–1174, Jul. 2004, doi: 10.1002/JCC.20035.

[47] J. Wang, W. Wang, P. A. Kollman, and D. A. Case, "Automatic atom type and bond type perception in molecular mechanical calculations," *J Mol Graph Model*, vol. 25, no. 2, pp. 247–260, Oct. 2006, doi: 10.1016/J.JMGM.2005.12.005.

[48] C. I. Bayly *et al.*, "A Second Generation Force Field for the Simulation of Proteins, Nucleic Acids, and Organic Molecules," *J Am Chem Soc*, vol. 117, no. 19, pp. 5179–5197, 1995, doi: 10.1021/JA00124A002.

[49] M. D. Hanwell, D. E. Curtis, D. C. Lonie, T. Vandermeerschd, E. Zurek, and G. R. Hutchison, "Avogadro: An advanced semantic chemical editor, visualization, and analysis platform," *J Cheminform*, vol. 4, no. 8, pp. 1–17, Aug. 2012, doi: 10.1186/1758-2946-4-17/FIGURES/14.

[50] M. Schudel, S. H. Behrens, H. Holthoff, R. Kretzschmar, and M. Borkovec, "Absolute Aggregation Rate Constants of Hematite Particles in Aqueous Suspensions: A Comparison of Two Different Surface Morphologies," *J Colloid Interface Sci*, vol. 196, no. 2, pp. 241–253, Dec. 1997, doi: 10.1006/JCIS.1997.5207.

[51] H. Sis and M. Birinci, "Effect of nonionic and ionic surfactants on zeta potential and dispersion properties of carbon black powders," *Colloids Surf A Physicochem Eng Asp*, vol. 341, no. 1–3, pp. 60–67, Jun. 2009, doi: 10.1016/J.COLSURFA.2009.03.039.

[52] W. F. Long and P. Labute, "Calibrative approaches to protein solubility modeling of a mutant series using physicochemical descriptors," *J Comput Aided Mol Des*, vol. 24, no. 11, pp. 907–916, Sep. 2010, doi: 10.1007/S10822-010-9383-Z/FIGURES/7.

[53] D. R. Grisham and V. Nanda, "Hydrodynamic radius coincides with the slip plane position in the electrokinetic behavior of lysozyme," *Proteins: Structure, Function, and Bioinformatics*, vol. 86, no. 5, pp. 515–523, May 2018, doi: 10.1002/PROT.25469.

[54] X. Liu, G. Qiu, A. Yan, Z. Wang, and X. Li, "Hydrothermal synthesis and characterization of α-FeOOH and α-Fe2O3 uniform nanocrystallines," *J Alloys Compd*, vol. 433, no. 1–2, pp. 216–220, May 2007, doi: 10.1016/J.JALLCOM.2006.06.029.

[55] S. B. Wang, Y. L. Min, and S. H. Yu, "Synthesis and magnetic properties of uniform hematite nanocubes," *Journal of Physical Chemistry C*, vol. 111, no. 9, pp. 3551–3554, Mar. 2007, doi: 10.1021/JP068647E/SUPPL_FILE/JP068647ESI20070127_043148.PDF.

[56] J. Ma, J. Lian, X. Duan, X. Liu, and W. Zheng, "α-Fe2O3: Hydrothermal synthesis, magnetic and electrochemical properties," *Journal of Physical Chemistry C*, vol. 114, no. 24, pp. 10671–10676, Jun. 2010, doi: 10.1021/JP102243G/SUPPL_FILE/JP102243G_SI_001.PDF.

[57] C. D. Zappielo *et al.*, "Solid Phase Extraction to On-Line Preconcentrate Trace Cadmium Using Chemically Modified Nano-Carbon Black with 3-Mercaptopropyltrimethoxysilane," *J Braz Chem Soc*, vol. 27, no. 10, pp. 1715–1726, Oct. 2016, doi: 10.5935/0103-5053.20160052.

[58] W. Lu *et al.*, "Synthesis and Applications of Graphene/Iron(III) Oxide Composites," *ChemElectroChem*, vol. 6, no. 19, pp. 4922–4948, Oct. 2019, doi: 10.1002/CELC.201901006.

[59] J. Zoubir, N. Bougdour, C. Radaa, A. Idlahcen, I. Bakas, and A. Assabbane, "Elaboration of a novel nanosensor using nanoparticles of α-Fe2O3 magnetic cores for the detection of metronidazole drug. Urine human and tap water," *Sensors International*, vol. 3, p. 100160, Jan. 2022, doi: 10.1016/J.SINTL.2022.100160.

[60] B. Xu *et al.*, "Iron oxide-based nanomaterials for supercapacitors," *Nanotechnology*, vol. 30, no. 20, p. 204002, Mar. 2019, doi: 10.1088/1361-6528/AB009F.

[61] A. J. Bard and L. R. Faulkner, "Polarography and Pulse Voltammetry," *Electrochemical Methods: Fundamentals and Applications*, pp. 261–304, Dec. 2001, Accessed: Jun. 18, 2024. [Online]. Available: https://www.wiley.com/en-us/Electrochemical+Methods%3A+Fundamentals+and+Applications%2C+2nd+Edition-p-9780471043720

[62] W. J. Yu, P. X. Hou, F. Li, and C. Liu, "Improved electrochemical performance of Fe2O3 nanoparticles confined in carbon nanotubes," *J Mater Chem*, vol. 22, no. 27, pp. 13756–13763, Jun. 2012, doi: 10.1039/C2JM31442H.

[63] J. Liu, H. Yang, and X. Xue, "Preparation of different shaped α-Fe2O3 nanoparticles with large particles of iron oxide red," *CrystEngComm*, vol. 21, no. 7, pp. 1097–1101, Feb. 2019, doi: 10.1039/C8CE01920G.

[64] D. Singh, S. Shaktawat, S. K. Yadav, R. Verma, K. R. Singh, and J. Singh, "Chitosan-assisted self-assembly of flower-shaped ε-Fe2O3 nanoparticles on screen-printed carbon electrode for Impedimetric detection of Cd2+, Pb2+, and Hg2+ heavy metal

ions in various water samples," *Int J Biol Macromol*, vol. 265, p. 130867, Apr. 2024, doi: 10.1016/J.IJBIOMAC.2024.130867.

[65] Z. Song *et al.*, "Preparation and electrochemical properties of Fe2O3/reduced graphene oxide aerogel (Fe2O3/rGOA) composites for supercapacitors," *J Alloys Compd*, vol. 685, pp. 355–363, Nov. 2016, doi: 10.1016/J.JALLCOM.2016.05.323.

[66] B. W. Ninham and V. A. Parsegian, "Electrostatic potential between surfaces bearing ionizable groups in ionic equilibrium with physiologic saline solution," *J Theor Biol*, vol. 31, no. 3, pp. 405–428, Jun. 1971, doi: 10.1016/0022-5193(71)90019-1.

[67] H. Sis and M. Birinci, "Effect of nonionic and ionic surfactants on zeta potential and dispersion properties of carbon black powders," *Colloids Surf A Physicochem Eng Asp*, vol. 341, no. 1–3, pp. 60–67, Jun. 2009, doi: 10.1016/J.COLSURFA.2009.03.039.

[68] M. Schudel, S. H. Behrens, H. Holthoff, R. Kretzschmar, and M. Borkovec, "Absolute Aggregation Rate Constants of Hematite Particles in Aqueous Suspensions: A Comparison of Two Different Surface Morphologies," *J Colloid Interface Sci*, vol. 196, no. 2, pp. 241–253, Dec. 1997, doi: 10.1006/JCIS.1997.5207.

[69] S. Koutsopoulos, K. Patzscly, W. T. E. Bosker, and W. Norde, "Adsorption of trypsin on hydrophilic and hydrophobic surfaces," *Langmuir*, vol. 23, no. 4, pp. 2000–2006, Feb. 2007, doi: 10.1021/LA062238S/ASSET/IMAGES/MEDIUM/LA062238SN00001.GIF.

[70] K. Brown *et al.*, "Utilization of an Electrochemiluminescence Sensor for Atropine Determination in Complex Matrices," *Anal Chem*, vol. 91, no. 19, pp. 12369–12376, Oct. 2019, doi: 10.1021/ACS.ANALCHEM.9B02905/ASSET/IMAGES/LARGE/AC9B02905_0007.JPEG.

[71] "Adsorptive Anodic Stripping Voltammetric Determination of Atropine in Urine Sample," 2021, doi: 10.1149/1945-7111/abe9cd.

[72] I. V. S. Arantes, R. D. Crapnell, M. J. Whittingham, E. Sigley, T. R. L. C. Paixão, and C. E. Banks, "Additive Manufacturing of a Portable Electrochemical Sensor with a Recycled Conductive Filament for the Detection of Atropine in Spiked Drink Samples," *ACS Applied Engineering Materials*, vol. 1, no. 9, pp. 2397–2406, Sep. 2023, doi: 10.1021/ACSAENM.3C00345.

[73] A. F. João, R. G. Rocha, T. A. Matias, E. M. Richter, J. Flávio S. Petruci, and R. A. A. Muñoz, "3D-printing in forensic electrochemistry: Atropine determination in beverages using an additively manufactured graphene-polylactic acid electrode,"

*Microchemical Journal*, vol. 167, p. 106324, Aug. 2021, doi: 10.1016/J.MICROC.2021.106324.